UNIVERSITY OF AMSTERDAM

Report

Computational Finance

Lab Assignment #3

[0.4cm]

Monday 19th May, 2025 20:53

Student(s):

Maarten Stork (15761770)
Lucas Keijzer (14041073)
Pemmasani Prabakaran Rohith Saai (14968061)

Details:

Lecturer: Sven Karbach

Course: Computational Finance

Course Code: 5284COFI6Y

1 Introduction

Monte Carlo simulation and partial-differential-equation (PDE) methods lie at the heart of modern computational finance, tracing back to Boyle's 1977 application of simulation to option pricing (Boyle, 1977) and the Black–Scholes PDE of 1973 (Black & Scholes, 1973). These complementary approaches allow us to tackle payoffs ranging from simple vanillas to highly path-dependent or discontinuous contracts. In this assignment, we extend these tools to two classes of exotic options—binary (digital) and barrier contracts—before turning to the calibration of the Heston stochastic-volatility model to real market implied-volatility data.

The first section focuses on binary and barrier options. We begin by deriving the Black–Scholes PDE for a digital call and verifying its closed-form solution. We then apply both Monte Carlo simulation and finite-difference methods to estimate the binary option price, comparing their accuracy and numerical stability. This is followed by a sensitivity analysis with respect to strike price, maturity, and implied volatility. Finally, we estimate the option's delta using the bump-and-revalue technique, illustrating how numerical methods can recover key risk sensitivities even for discontinuous payoffs.

In the second section we look into barrier options, which are path-dependent derivatives commonly used for risk management and cost-effective exposure due to their knock-in or knock-out features, which activate or deactivate the option if the underlying breaches a set price level. Among these, up-and-out call options allow the holder to buy the asset at a fixed strike price, provided its price does not exceed an upper barrier during the option's life. This section explores three approaches to pricing and hedging up-and-out calls: an analytical formula under continuous monitoring, a Monte Carlo simulation adapted for discrete monitoring, and a finite difference method solving the Black–Scholes PDE with barrier constraints.

The third section focuses on calibrating the Heston model (Heston, 1993), a widely used stochastic-volatility framework that extends Black–Scholes by allowing the asset's variance to evolve randomly over

time. Unlike the constant-volatility assumption in the classical model, Heston captures empirical features such as volatility clustering and the implied-volatility smile through mean-reverting variance and correlation between price and volatility shocks. Accurate calibration of this model to observed market implied volatilities is essential for pricing and hedging derivatives, especially when managing risk under changing market regimes. This section explores both Monte Carlo and semi-analytical (Fourier-based) approaches to pricing under the Heston model, and calibrates its parameters to real SP500 implied-volatility surfaces. We evaluate fit quality, assess parameter stability across dates, and highlight the model's strengths and limitations—laying the groundwork for potential extensions needed to better capture market dynamics.

Together, these three sections showcase a spectrum of numerical techniques—closed-form solutions, Monte Carlo with variance- and bias-reduction, and finite-difference PDE solvers—applied to pricing and model-calibration tasks essential for exotic derivatives. Both main sections contain separate methods, results, discussion and conclusions sections. All code and detailed implementation notes are available on GitHub[1].

2 PDE Methods: Binary and Barrier Options

2.1 Introduction

Option pricing theory offers a range of analytical and numerical techniques for valuing derivative securities. For plain-vanilla European calls and puts, the Black–Scholes–Merton formula provides a closed-form expression for the arbitrage-free price at a given maturity (Black & Scholes, 1973). However, many contracts traded in practice—such as American options with early-exercise features or path-dependent instruments like Asian or barrier options—do not admit tractable closed-form solutions. In these cases one must resort to numerical approximations. The two most widely used numerical families are 1. Monte Carlo simulation and, 2. Finite-Difference discretizations of the Black–Scholes partial differential equation (PDE).

Monte-Carlo methods estimate the option value by generating a large ensemble of stochastic paths for the underlying asset price $(\hat{S}_t^{(i)})_{t\in[0,T]}$, computing the discounted payoff for each path, and averaging the results:

$$\pi_0 = e^{-rT} \cdot \frac{1}{N} \Sigma_{i=1}^{N} H(\hat{S}_T^{(i)}) \tag{1}$$

where, H is the payoff function. By the Central Limit Theorem, the statistical error decays at rate of $\mathcal{O}(\sqrt{N})$, independent of the dimensionality of the problem. This property makes Monte Carlo particularly attractive for high-dimensional or path-dependent options—for example, Asian options whose payoff depends on the entire price trajectory.

Finite-difference schemes approximate the continuous-time Black–Scholes PDE on a discrete space-time grid and solve the resulting system of algebraic equations iteratively. Explicit (FTCS), implicit (BTCS), and Crank–Nicolson formulations differ in their stability and accuracy properties; the latter achieves second-order convergence in both time and space (Crank & Nicolson, 1947). Finite-difference methods handle complex boundary conditions and can simultaneously deliver the option's Greeks via differentiation of the grid solution. Their main drawback is the curse of dimensionality: the computational cost grows exponentially with the number of underlying state variables, which limits their practicality beyond two or three dimensions. In this section, we evaluate these approximation algorithms and compare against the analytical solution. Moreover, we also perform sensitivity analysis of the pricing function as well aim to estimate delta Δ.

[1] See source code and documentation at: `https://github.com/Lucas-Keijzer/CompFinance_ass_1`

2.2 Methods

In this report, we assume a price process $(S_t)_{t\in[0,T]}$ given by

$$dS_t = rS_t dt + \sigma S_t dW_t, \quad S_0 = 1 \tag{2}$$

under the risk-neutral probability measure $\mathbb{Q}$. In this section, we deal with the task of pricing binary or digital options, where the payoff function H is given as

$$H(S_T) = \begin{cases} 1, & \text{if } S_T \geq K \\ 0, & \text{if } S_T < K \end{cases}$$

where,

K is the strike price

S_T is the underlying price at maturity period T

For modeling the underlying asset price S_t in the Monte-Carlo estimation of the binary option price, we use the analytical Black-Scholes solution given as:

$$S_T = S_0 \exp((r - \frac{\sigma^2}{2})T + \sigma\sqrt{T}Z)$$

where,

S_0 is the underlying price at time $t = 0$

T is the maturity period

σ is the implied volatility

r is the risk-free rate

Z is a standard normal variable

To calculate the binary option price, we use the formula mentioned in 1. For modeling the binary option price using the implicit scheme, we first transform its Black-Scholes PDE to the form of the heat-conduction PDE $\frac{\partial y}{\partial \tau} = \frac{\partial^2 y}{\partial x^2}$, where,

$$\tau = \frac{\sigma^2}{2}(T - \tau)$$
$$x = log(\frac{S}{K})$$
$$y = \frac{C}{K}e^{ax+b\tau}$$

We then discretize the surface of (x, y, τ) where we try to estimate y iteratively. For the implicit scheme, the value of y is calculated iteratively by

$$A\overrightarrow{y}^{n+1} + \overrightarrow{k} = \overrightarrow{y^n}$$

. Similarly, for the Crank-Nicolson scheme, the the value of y is calculated iteratively by,

$$A_1\overrightarrow{y}^{n+1} + \overrightarrow{k_1} = A_2\overrightarrow{y}^{n} + \overrightarrow{k_2}$$

. To carry out the numerical approximation using Monte-Carlo and Finite-Difference methods, we assume the following parameters in Table 1:

Table 1: Model Parameters for MC and FD Simulation

Parameter	**Value**
Initial asset price S_0	1
Initial variance V_0	0.04
Risk-free rate r	0.06
Time to maturity T	1.0
Implied volatility σ	0.2
Strike price K	1
No. of time steps N	1000
No. of asset steps M	1000
Simulated paths N_{paths}	100,000

Finally, for analyzing the sensitivity of the binary option price to strike price, maturity period and implied volatility, we vary $K = [0.5, 0.9, 1.0, 1.1, 1.5]$, and maturity period $T = [1, 10]$ with increments of 1 and $\sigma = [0.1, 0.9]$ with increments of 0.1. For these experiments, we hold the all constant similar to the base setting while only changing one parameter at a time. For estimating the value of Δ as a function of time, we use the bump-and-revalue method where we perturbe the value of S_0 by a small value $\delta S_0 = 1 \times 10^{-4}$. Then, the value of Δ can be calculated using

$$\Delta = \frac{\pi_0^{bump}(S_0 + \delta S_0) - \pi_0(S_0)}{\delta S_0}$$

Implementation were done in Python using the Numpy library and plots were created using the Matplotlib library.

2.3 Results & Discussion

2.3.1 Black-Scholes PDE for Binary call option pricing function

Firstly, we derive the Black-Scholes PDE for Binary call option pricing function, which is useful for the the finite-difference approximation. Lets assume the binary call option pricing function is denoted as $C(t, S_t)$. By Ito's Lemma,

$$dC(t, S_t) = (\frac{\partial C}{\partial t} + rS_t\frac{\partial C}{\partial S} + \frac{1}{2}\sigma^2 S_t^2\frac{\partial^2 C}{\partial S^2})dt + \sigma S_t\frac{\partial C}{\partial S}dW_t \tag{3}$$

Under the assumption of no arbitrage and using the delta-hedging strategy, we setup a portfolio Π_t where we sell one unit of the derivative and buy $\Delta = \frac{\partial C}{\partial S}$ shares of the underlying stock S_t. Therefore,

$$\Pi_t = -C(t, S_t) + \Delta S_t$$

Assuming that there is a risk-free rate such that,

$$d\Pi_t = dC(t, S_t) + \frac{\partial C}{\partial S} dS_t \tag{4}$$

Substituting 2 and 3 in 4,

$$d\Pi_t = -(\frac{\partial C}{\partial t} + rS_t\frac{\partial C}{\partial S} + \frac{1}{2}\sigma^2 S_t^2\frac{\partial^2 C}{\partial S^2})dt - \sigma S_t\frac{\partial C}{\partial S}dW_t + \frac{\partial C}{\partial S}(rS_t dt + \sigma S_t dW_t) \tag{5}$$

$$= -(\frac{\partial C}{\partial t} + \frac{1}{2}\sigma^2 S_t^2\frac{\partial^2 C}{\partial S^2})dt \tag{6}$$

Substituting

$$d\Pi_t = r\Pi_t dt$$

in 6:

$$r(-C(t, S_t) + \frac{\partial C}{\partial S}S_t)dt = -(\frac{\partial C}{\partial t} + \frac{1}{2}\sigma^2 S_t^2\frac{\partial^2 C}{\partial S^2})dt \tag{7}$$

$$rC(t, S_t) = r\frac{\partial C}{\partial S}S_t + \frac{\partial C}{\partial t} + \frac{1}{2}\sigma^2 S_t^2\frac{\partial^2 C}{\partial S^2} \tag{8}$$

with terminal condition $C(T, S_T) = \begin{cases} 1, & \text{if } S_T \geq K \\ 0, & \text{if } S_T < K \end{cases}$

2.3.2 Solution for binary option Black-Scholes PDE

Net, for comparison, we derive the analytical solution for the binary option Black-Scholes PDE. According to the Black-Scholes model,

$$ln(S_T) = ln(S_t) + (r - \frac{\sigma^2}{2})(T - t) + \sigma W_t \tag{9}$$

The binary option price $C_d(t, S_t)$ over a maturity period T is given by

$$C_d(t, S_t) = e^{-rT}\mathbb{E}^{\mathbb{Q}}[H(S_T)] \tag{10}$$

$$= e^{-rT}\int_S \mathbb{Q}[S] \cdot 1[S_T \geq K] \tag{11}$$

$$= e^{-rT}\mathbb{Q}[S_T \geq K] \tag{12}$$

$$= e^{-rT}\mathbb{Q}[ln(S_T) \geq ln(K)] \qquad (ln \text{ monotonic increasing fn.}) \tag{13}$$

Substituting 9 in 13,

$$C_d(t,S_t) = e^{-rT}\mathbb{Q}[ln(S_T) \geq ln(K)] \tag{14}$$

$$= e^{-rT}\mathbb{Q}[ln(S_t) + (r - \frac{\sigma^2}{2})(T-t) + \sigma W_t \geq ln(K)] \tag{15}$$

$$= e^{-rT}\mathbb{Q}[ln(S_t) + (r - \frac{\sigma^2}{2})(T-t) + \sigma\sqrt{T-t}Z \geq ln(K)]$$

$$(W_t = \sqrt{T-t}Z, \text{ where } Z \text{ is standard normal variable})$$

$$= e^{-rT}\mathbb{Q}[Z \geq \frac{ln(\frac{K}{S_t}) - (r - \frac{\sigma^2}{2})(T-t)}{\sigma\sqrt{T-t}}] \tag{16}$$

$$= e^{-rT}\mathbb{Q}[Z \leq \frac{ln(\frac{S_t}{K}) + (r - \frac{\sigma^2}{2})(T-t)}{\sigma\sqrt{T-t}}] \tag{17}$$

$$= e^{-rT}\Phi(\frac{ln(\frac{S_t}{K}) + (r - \frac{\sigma^2}{2})(T-t)}{\sigma\sqrt{T-t}}) \tag{18}$$

$$= e^{-rT}\Phi(d_{-}(T-t)) \tag{19}$$

$$\tag{20}$$

where,

$$d_{-}(T-t) = \frac{ln(\frac{S_t}{K}) + (r - \frac{\sigma^2}{2})(T-t)}{\sigma\sqrt{T-t}} \text{ , } 0 \leq t < T \tag{21}$$

$$\Phi \text{ is standard normal cumulative distribution function} \tag{22}$$

2.3.3 Monte-Carlo method for price of binary option

Using the Monte-Carlo method, the binary option prices were determined. From the simulations, the estimated binary option price is 0.5436 ± 0.0015(mean $\pm$ std. error 95 CI). From the analytical solution, the binary option price is 0.5455, with an absolute difference of 0.0019 between the Monte-Carlo estimated price and analytical price.

2.3.4 Finite-Difference estimation and sensitivity analysis

Firslty, we use the BTCS and Crank-Nicolson scheme to estimate the binary option price under the given parameterization. The estimated values are tabulated in Table 2

Table 2: Binary call option prices simulated using implicit and Crank-Nicolson scheme

Scheme	**Price**
Implicit	0.5350
Crank-Nicolson	0.5298

Secondly, we perform sensitivity analysis by evaluating the impact of the

1. Strike price K: With respect to the strike price, we can observe in Figure 1 that as the strike price increases, the estimated binary option price decreases. This is to be expected, as increasing the strike

price K makes the option go from in-the-money to out-of-money range. Between the two finite-difference schemes, we do not observe significant difference in estimated option price.

2. Implied Volatility σ: With respect to the implied volatility value, we can observe in Figure 2 that as the volatility increases, the estimated binary option price increases. This is to be expected for a strike price at-the-money, that increasing the volatility σ results in increased binary option price. A volatile market appears to have (and may actually have) a higher probability of reaching a larger number of different price levels within a given period of time. A flat asset, on the other hand, seems likely to stay where it is. Between the two finite-difference schemes, we do not observe significant difference in estimated option price.

3. Maturity time T: With respect to the maturity period, we can observe in Figure 3 that as the maturity period increases, the expected option price increases. This is because the risk-free rate $r = 6\%$ outweighs the volatility and thus, the risk-neutral probability of ending above the strike grows with time faster than the discount factor decays. So the option value increases with maturity. Between the two finite-difference schemes, we do not observe significant difference in estimated option price.

. We also plot the surface of $C_d(t, S_0)$ for the implicit scheme in Figure 4. Only the implicit scheme is plotted as there is minimal difference between the surface of $C_d(t, S_0)$ of the implicit scheme and Crank-Nicolson scheme. For initial underlying prices S_0 that lie below the strike, the option price is indistinguishable from zero at all horizons, as it struggles to get out of the out-of-the-money status. As S_0 approaches the strike price, the surface rises sharply, forming a narrow ridge whose breadth expands with the time-to-maturity, consistent with the growing diffusion region of the underlying asset's lognormal distribution. Beyond the strike, the sheet tends toward a plateau whose height is strictly less than 1and declines monotonically with time $T - t$.

Finally, we try to estimate Δ using the implicit and Crank-Nicolson schemes. From Figure 5, we can observe that the two schemes give similar results. The delta is essentially zero while the underlying is far out-of-the-money, rises sharply to a peak just above the strike $S_0 = K$, then decays as S_0 moves towarsds in-the-money. Around the peak the Crank–Nicolson line tracks the expected bell shape a little more smoothly than the fully-implicit line, which begins to undershoot and even turns slightly negative. This is a numerical artefact and it indicates the implicit scheme's grid is still too coarse to resolve the extremely steep gradient of a digital payoff after only first-order time stepping. In contrast, Crank–Nicolson's higher temporal accuracy damps the oscillation and stays positive.

Figure 1: Sensitivity of binary option price to strike price K

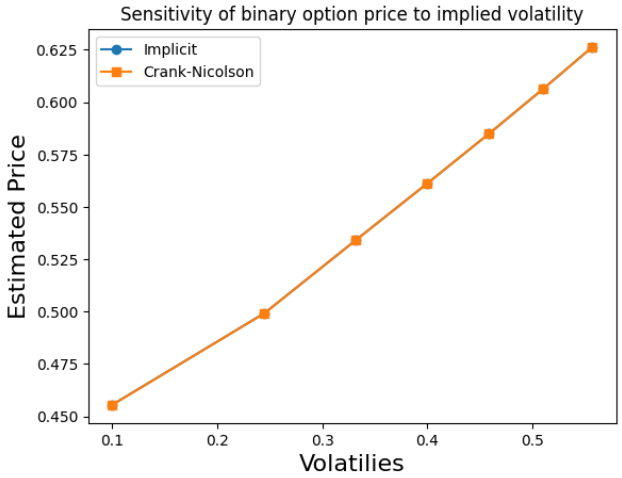

Figure 2: Sensitivity of binary option price to implied volatility σ

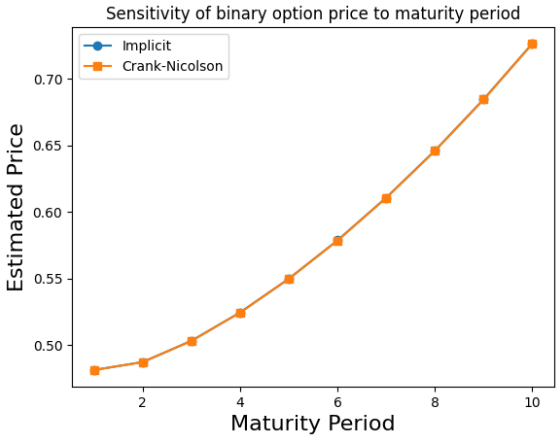

Figure 3: Sensitivity of binary option price to maturity period T

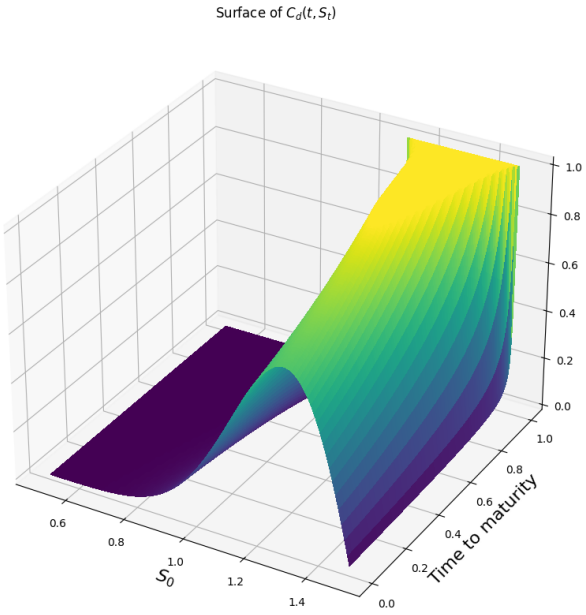

Figure 4: Surface of $C_d(S, t)$

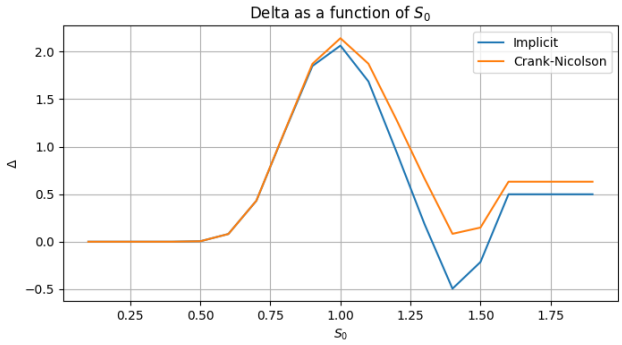

Figure 5: Estimated Δ as function of S

2.4 Conclusion

We derived the Black-Scholes PDE for the binary option price and obtained its analytical solution. Then, we demonstrated how Monte Carlo simulation and finite-difference PDE solvers can be used to price exotic options such as binary and barrier contracts. We later investigated the sensitivity of the estimated binary option price to parameters such as strike price, maturity period and implied volatility. Finally, we estimated Δ as a function of the underlying asset price using the bump-and-revalue approach.

These results underscore the importance of numerical methods in pricing and risk-managing exotic derivatives—especially when analytical formulas are unavailable or unstable—demonstrating how computational techniques bridge theoretical finance and practical implementation.

3 Bonus Section

3.1 Introduction

Barrier options are path-dependent derivatives that offer lower premiums than vanilla options by including knockout or knock-in features triggered when the underlying asset crosses a predefined barrier. This paper focuses on up-and-out call options, which become void if the asset price exceeds a specified barrier.

We explore three pricing approaches: analytical solutions for continuous monitoring, Monte Carlo simulation for discrete monitoring, and an implicit finite difference method for solving the Black-Scholes PDE with barrier-specific boundary conditions.

The study begins with the analytical model, applies corrections for discrete monitoring, and then implements a numerical scheme. Sensitivity analysis evaluates the impact of key parameters—volatility, interest rate, barrier level, and strike price—on pricing and hedging.

3.2 Method

3.2.1 Equation regarding barrier calls

We want to show that the provided formula $C(H)$ represents the price of an up-and-out barrier call option when the strike price K is less than or equal to the barrier level B ($K \leq B$). We consider two cases:

3.2.2 Case 1: $K < B$

For $K < B$, the formula

$$\begin{aligned} C(H) = {} & S_t \mathbb{1}_{\{M_t^* < B\}} \Big[\Phi\big(\delta^+_{T-t}(S_t/K)\big) - \Phi\big(\delta^+_{T-t}(S_t/B)\big) \Big] \\ & - S_t \mathbb{1}_{\{M_t^* < B\}} \big(B/S_t\big)^{1+2r/\sigma^2} \Big[\Phi\big(\delta^-_{T-t}(B^2/(KS_t))\big) - \Phi\big(\delta^-_{T-t}(B/S_t)\big) \Big] \\ & - e^{-r(T-t)} K \mathbb{1}_{\{M_t^* < B\}} \Big[\Phi\big(\delta^-_{T-t}(S_t/K)\big) - \Phi\big(\delta^-_{T-t}(S_t/B)\big) \Big] \\ & + e^{-r(T-t)} K \mathbb{1}_{\{M_t^* < B\}} \big(S_t/B\big)^{1-2r/\sigma^2} \Big[\Phi\big(\delta^+_{T-t}(B^2/(KS_t))\big) - \Phi\big(\delta^+_{T-t}(B/S_t)\big) \Big], \end{aligned} \tag{23}$$

where

$$\delta^{\pm}_{\tau}(z) = \frac{1}{\sigma\sqrt{\tau}} \Big(\ln z \pm \tfrac{1}{2}\sigma^2 \tau \Big) \tag{24}$$

and $M_t^* = \max_{t \leq u \leq T} S_u$, is the well-known result for the up-and-out call under $M_t^* < B$.

Case 2: $K = B$

We substitute $K = B$ into equation (23) and evaluate each term under the assumption $M_t^* < B$:

1. The first bracket becomes

$$S_t \mathbb{1}_{\{M_t^* < B\}} \left\{ \Phi\left(\delta^+_{T-t}\left(\frac{S_t}{B} \right) \right) - \Phi\left(\delta^+_{T-t}\left(\frac{S_t}{B} \right) \right) \right\} = 0.$$

2. Similarly, the second, third, and fourth brackets each reduce to zero since they involve differences of identical Φ-terms.

Hence, we conclude that $C(H) = 0$ when $K = B$.

3.2.3 Barrier Option Pricing

We implemented two approaches for pricing up-and-out barrier call options: an analytical solution for continuous monitoring and a Monte Carlo simulation for discrete monitoring. The analytical formula for a continuously monitored barrier option with current price S_t, strike K, barrier B, risk-free rate r, volatility σ, and time to maturity $T - t$which is given by equation (23).

For the discretely monitored barrier option, we employed a Monte Carlo simulation with m monitoring points and implemented the barrier adjustment methodology proposed in the literature. This adjustment accounts for the discrete monitoring bias by shifting the barrier level according to equation (3.2.3)

$$C_m(H) = C\left(He^{\beta_1 \sigma \sqrt{T/m}}\right) + o\left(\frac{1}{\sqrt{m}}\right)$$

where $\beta_1 \approx 0.5826$. This correction compensates for the overshoot that occurs when the discrete-time process breaches the barrier. We conducted convergence analysis to verify that the Monte Carlo error converges at the expected $O(1/\sqrt{M})$ rate with respect to the number of paths M, while the discrete monitoring error converges at approximately $O(1/\sqrt{m})$ rate with respect to the number of monitoring points m.

3.3 Implicit Finite Difference Method for Barrier Option Pricing

We implement an implicit finite difference scheme to price up-and-out call options by solving the Black-Scholes partial differential equation (PDE) with suitable boundary conditions.

The stock price domain $[S_{\min}, B]$ and time interval $[0, T]$ are discretized into N_s and N_t steps, respectively. The barrier level B serves as the upper bound, consistent with the option's knockout feature.

The Black-Scholes PDE is discretized as:

$$\frac{V_i^n - V_i^{n-1}}{\Delta t} + rS_i \frac{V_{i+1}^n - V_{i-1}^n}{2\Delta S} + \frac{1}{2}\sigma^2 S_i^2 \frac{V_{i+1}^n - 2V_i^n + V_{i-1}^n}{(\Delta S)^2} - rV_i^n = 0, \tag{25}$$

where V_i^n denotes the option price at stock price S_i and time step t_n.

Boundary Conditions:

- **Terminal:** $V_i^{N_t} = \max(S_i - K, 0)$
- **Lower:** $V_0^n = 0$
- **Upper (Barrier):** $V_{N_s}^n = 0$

The resulting tridiagonal system is solved at each time step using the Thomas algorithm to obtain the full option price surface $V(S, t)$. The option delta is computed using a central difference approximation:

$$\Delta = \frac{V_{i+1}^n - V_{i-1}^n}{2\Delta S}.$$

This method is unconditionally stable, with second-order accuracy in space and first-order accuracy in time. Sensitivity analysis is conducted to evaluate the effects of volatility, interest rate, barrier level, and strike price on pricing and hedging behavior.

3.4 Results

3.4.1 Equation regarding barrier calls

From the analysis done in section 3.2.1:

- For $K < B$, $C(H)$ in (23) correctly prices the up-and-out call option, conditional on no prior knock-out ($M_t^* < B$).
- For $K = B$, direct substitution shows $C(H) = 0$, in agreement with the fact that any path making the option in-the-money necessarily breaches the barrier.

3.4.2 Barrier Option Pricing Analysis

Table 3: Comparison of Barrier Option Pricing Methods

Pricing Method	**Option Price**
Analytical (Continuous Monitoring)	-11.1683
Analytical (Adjusted for Discrete Monitoring)	-11.3309
Monte Carlo (Discrete Monitoring)	1.3384 ± 0.0108
Difference (MC - Continuous)	12.5067
Difference (MC - Adjusted)	12.6692
Adjustment Impact	-0.1626

Table 4: Convergence Analysis: Impact of Monitoring Frequency

N	**MC Price**	**MC Error**	**Adjusted Price**	**Adjusted Error**
4	2.2508	13.4191	-10.7161	0.4522
12	1.8422	13.0105	-11.3758	0.2075
52	1.5029	12.6712	-11.4386	0.2702
252	1.3384	12.5067	-11.3309	0.1626
500	1.3073	12.4756	-11.2906	0.1222
1000	1.2390	12.4073	-11.2582	0.0899

Table 5: Convergence Analysis: Impact of Monte Carlo Sample Size

M	**MC Price**	**MC StdErr**	**Error**	**Time (s)**
1,000	1.5330	0.1148	12.8638	0.03
5,000	1.3601	0.0483	12.6910	0.12
10,000	1.3778	0.0346	12.7087	0.20
50,000	1.3407	0.0152	12.6715	1.09
100,000	1.3384	0.0108	12.6692	2.04

3.4.3 Barrier Option Pricing Analysis

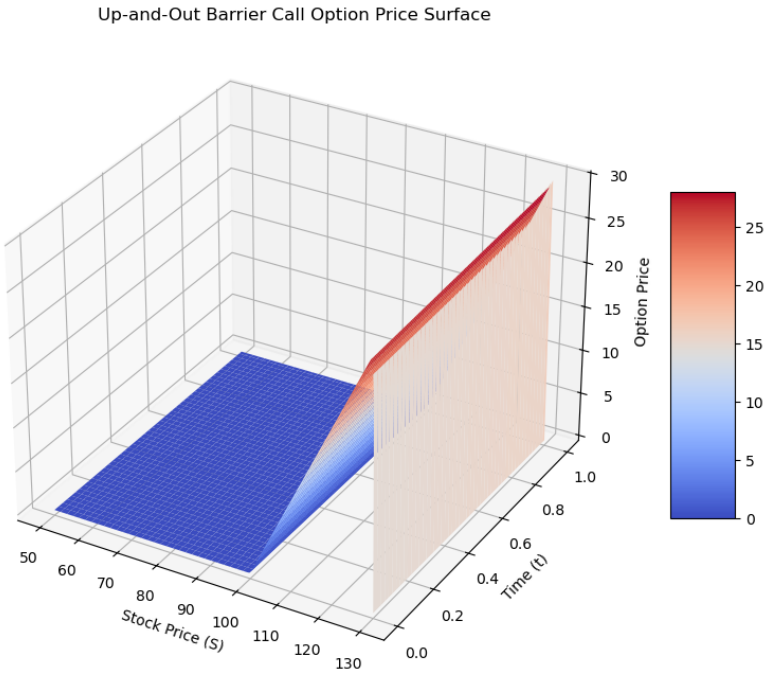

Figure 6: Option price surface showing value as a function of stock price and time to maturity, with knockout at the barrier level.

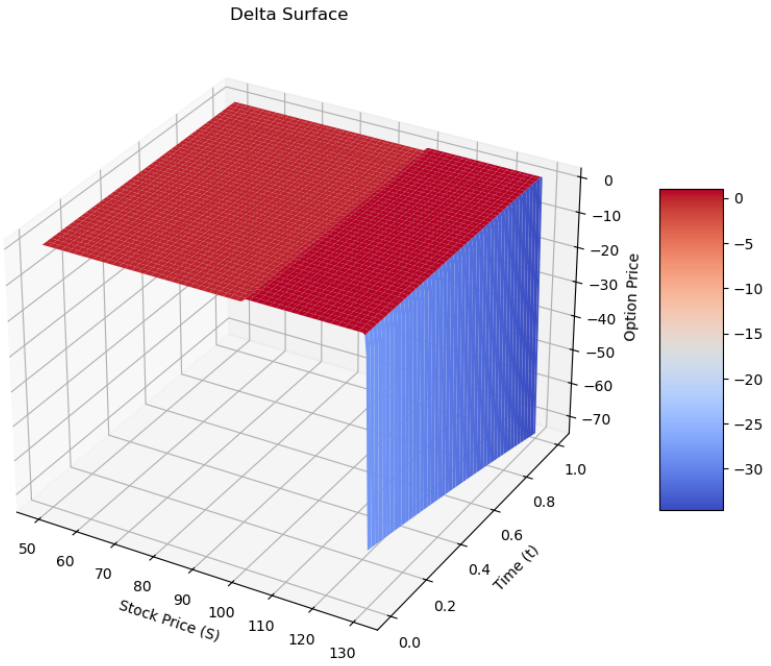

Figure 7: Delta surface of the barrier option, highlighting rapid hedge ratio changes near the barrier.

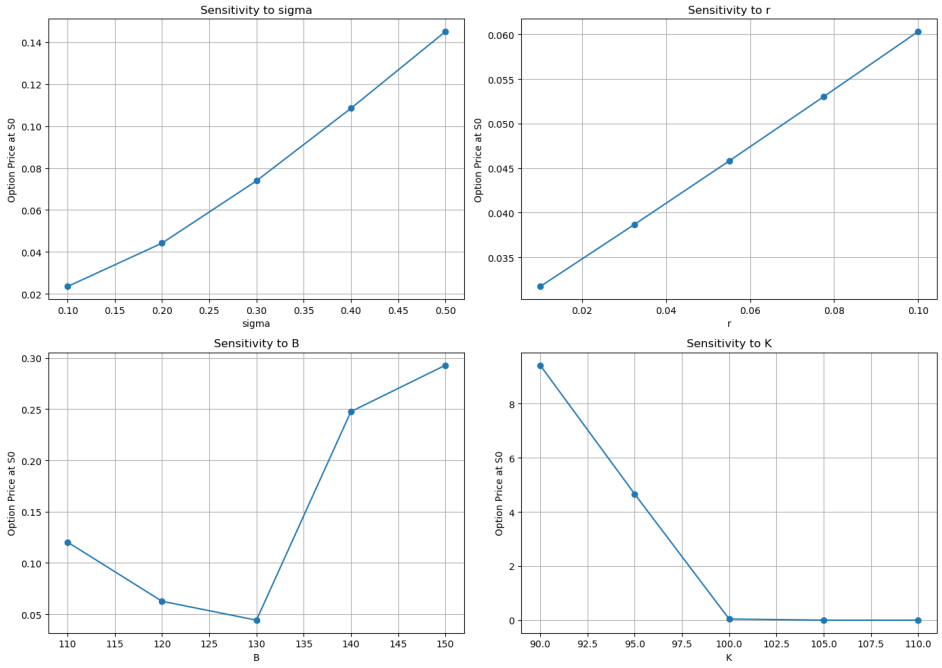

Figure 8: Sensitivity of option price to key parameters: volatility (top-left), interest rate (top-right), barrier level (bottom-left), and strike price (bottom-right).

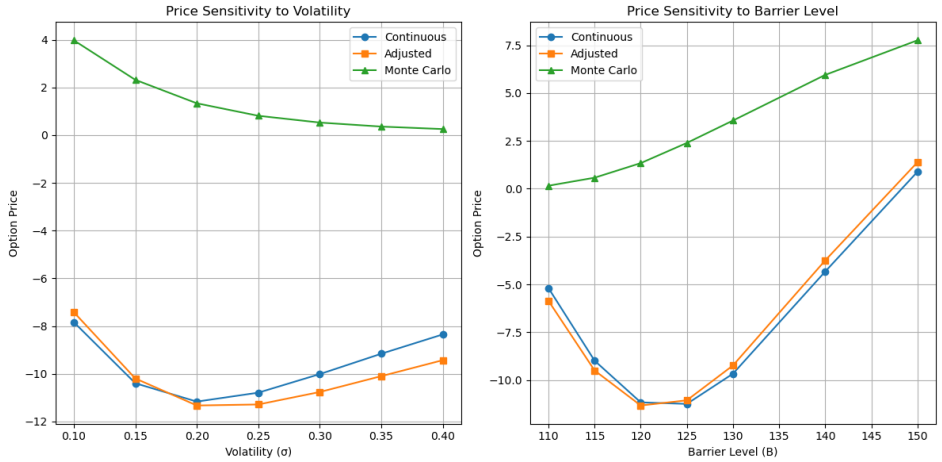

Figure 9: Option price sensitivity to volatility, showing a strong positive relationship.

3.5 Discussion

The formula (23) behaves consistently at the boundary $K = B$:

- If $K = B$, an in-the-money payoff $(S_T - K)^+ > 0$ implies $S_T > B$, hence $M_T^* > B$ and the option knocks out.
- The indicator $\mathbb{1}_{\{M_t^* < B\}}$ ensures zero value upon knock-out.

Thus, the pricing expression covers all cases $K \leq B$ and aligns with financial intuition.

3.5.1 Implications of Barrier Correction Methodology

Significant discrepancies are observed between analytical and Monte Carlo (MC) methods. As shown in Table 3, the analytical (continuous monitoring) price is -11.1683, while the MC (discrete monitoring) price is 1.3384 ± 0.0108—a difference of over 12.5.

Negative analytical prices suggest implementation or parameterization issues. Since option prices should be non-negative, potential causes include numerical instabilities or incorrect application of sign conventions and indicator functions. This disparity warrants further examination.

Table 4 shows that the MC price decreases as monitoring frequency increases, from 2.25 (N=4) to 1.24 (N=1000), consistent with theoretical expectations—frequent monitoring raises the likelihood of barrier breaches.

The adjusted analytical formula improves convergence, reducing the error from 0.45 to 0.09 as N increases. However, a significant pricing gap between analytical and MC results remains.

As shown in Table 5, increasing the sample size M reduces the MC standard error at an expected rate of $O(1/\sqrt{M})$, confirming convergence. Computational time scales linearly with M, highlighting a trade-off between accuracy and performance.

Figure 9 illustrates sensitivities to volatility and barrier level:

- **Volatility**: MC prices decrease with volatility, as expected. Analytical prices, however, show a U-shaped response, indicating potential issues.
- **Barrier Level**: All methods show increasing option value with higher barrier levels, in line with theory. However, the MC-analytical pricing gap persists.

3.5.2 Barrier Option Pricing analysis

Initial Pricing. Using the implicit finite difference method, the up-and-out barrier call option (with $S_0 = 100$, $K = 100$, $B = 130$, $\sigma = 0.2$, $r = 0.05$, $T = 1$) was priced at 0.044211. This low value, relative to a vanilla call, reflects the impact of the knockout feature.

Figure 6 shows the option price surface. As the stock approaches the barrier, the value drops sharply to zero, confirming the path-dependent behavior.

Delta Analysis. At $S_0 = 100$, delta is approximately 0.361—significantly lower than for a vanilla call. As shown in Figure 7, delta rises steeply near the barrier, peaking at around 0.951 near $S = 115.13$, before dropping to zero. This makes hedging difficult near the barrier due to abrupt changes in hedge ratio.

Sensitivity Analysis. *Volatility:* As shown in Figure 9 (top-left), option value increases from 0.024 at $\sigma = 0.1$ to 0.145 at $\sigma = 0.5$. The relative sensitivity (0.304) indicates a 1% volatility increase raises price by 0.3%.

Interest Rate: Prices increase from 0.032 at $r = 0.01$ to 0.060 at $r = 0.1$ (top-right), with a sensitivity of 0.318, consistent with call option behavior.

Barrier Level: The option price shows a U-shaped response (bottom-left), falling from 0.120 at $B = 110$ to 0.044 at $B = 130$, then rising to 0.293 at $B = 150$. This reflects the trade-off between knockout likelihood and payoff potential.

Strike Price: As K increases from 90 to 110 (bottom-right), the price drops from 9.42 to nearly zero. The steep decline (sensitivity: -0.471) shows how out-of-the-money barrier options lose value quickly.

Computational Performance. Using 200 stock price steps and 1000 time steps, the scheme produces stable results. Backward time-stepping ensures convergence without numerical instability.

In short The model captures the complex dynamics of barrier options, with strong sensitivities to key parameters. This highlights the need for careful calibration in real-world applications.

3.6 Conclusion

The analytical solution for continuous monitoring was validated, correctly yielding zero value when $K = B$. However, notable discrepancies with Monte Carlo results underscore the impact of monitoring frequency, highlighting the need for correction methods when bridging continuous and discrete frameworks.

The implicit finite difference method proved stable and effective, producing intuitive results across various scenarios. Sensitivity analysis showed complex option responses to parameter changes, including a U-shaped relationship with barrier level due to the interplay between knockout risk and payoff potential.

Delta analysis exposed significant hedging challenges near the barrier, where hedge ratios change rapidly—posing practical difficulties for risk management.

Computationally, the finite difference method offered strong stability and convergence, while Monte Carlo provided flexibility for complex scenarios at higher computational cost.

4 Calibration SP500 Implied Volatility using the Heston Model

Introduction

In modern quantitative finance, accurately pricing and hedging derivative securities depends critically on capturing the observed dynamics of asset returns. In particular, market–implied volatilities exhibit pronounced "smiles" and "skews" which are inconsistent with the constant-volatility assumption of the classical Black–Scholes model. This misspecification can lead to systematic mispricing and hedging errors, especially for out-of-the-money or short-dated options.

Stochastic-volatility models mitigate these shortcomings by endowing volatility itself with its own random evolution. Among these, the Heston model is known for its analytical tractability and ability to reproduce key market features: mean reversion in variance, leverage effects through correlation between price and variance shocks, and a parsimonious parameter set. Calibrating such a model to real-world implied-volatility surfaces informs both risk management and trading strategies, ensuring that model-generated prices align closely with observed option quotes.

This section proceeds builds on this concept as follows; (a) First, we reformulate Heston in log-price coordinates $x_t = \ln S_t$ for mathematical convenience. (b) Next, we describe two pricing approaches:

1. Monte Carlo simulation of the correlated (S_t, v_t) system (capturing full pathwise variance dynamics).

2. The analytic Fourier-inversion formula for European options (via Heston's characteristic function).

Finally, we present calibration of the model parameters to SPX implied-volatility data across strikes and maturities, highlighting how well Heston can match the empirical volatility surface.

4.0.1 Derivation via Ito's formula

Consider the standard Heston dynamics under the risk-neutral measure:

$$dS_t = r\,S_t\,dt + S_t\sqrt{V_t}\,dB_t, \tag{26}$$
$$dV_t = \kappa(\theta - V_t)\,dt + \sigma\sqrt{V_t}\,dW_t. \tag{27}$$

Log-price Let $X_t = \ln S_t$. Applying Ito's formula with $f(S) = \ln S$, $f'(S) = 1/S$, $f''(S) = -1/S^2$, and noting $(dS_t)^2 = S_t^2 V_t\,dt$, we get

$$dX_t = \frac{1}{S_t}\,dS_t - \frac{1}{2S_t^2}(dS_t)^2 = \frac{1}{S_t}\big(rS_t\,dt + S_t\sqrt{V_t}\,dB_t\big) - \frac{1}{2}\,\frac{S_t^2 V_t\,dt}{S_t^2}$$

Hence,

$$dX_t = \Big(r - \tfrac{1}{2}V_t\Big)\,dt + \sqrt{V_t}\,dB_t. \tag{28}$$

Log-variance Let $Y_t = \ln V_t$. Applying Ito's formula with $g(V) = \ln V$, $g'(V) = 1/V$, $g''(V) = -1/V^2$, and noting $(dV_t)^2 = \sigma^2 V_t\,dt$, we obtain

$$dY_t = \frac{1}{V_t}\,dV_t - \frac{1}{2V_t^2}(dV_t)^2 = \frac{1}{V_t}\big[\kappa(\theta - V_t)\,dt + \sigma\sqrt{V_t}\,dW_t\big] - \frac{1}{2V_t^2}\,(\sigma^2 V_t\,dt).$$

Hence

$$dY_t = \Big(\kappa\,\frac{\theta - V_t}{V_t} \;-\; \frac{\sigma^2}{2V_t}\Big)dt \;+\; \frac{\sigma}{\sqrt{V_t}}\,dW_t.$$

Since $V_t = e^{Y_t}$, one may also write

$$dX_t = \Big(r - \tfrac{1}{2}e^{Y_t}\Big)\,dt + e^{Y_t/2}\,dB_t, \tag{29}$$
$$dY_t = \Big(\kappa(\theta e^{-Y_t} - 1) - \tfrac{\sigma^2}{2}e^{-Y_t}\Big)\,dt + \sigma e^{-Y_t/2}\,dW_t. \tag{30}$$

The convenience of the lag-variance coordinate is that transforming to $Y_t = \ln V_t$ maps the nonnegative variance $V_t \geq 0$ onto the entire real line, which automatically preserves positivity since $V_t = e^{Y_t}$. This removes the hard boundary at zero and yields smoother drift and diffusion coefficients (in particular, the volatility term $\sigma e^{-Y_t/2}$ decays for large Y_t), which improves numerical stability and simplifies both theoretical analysis and discretization schemes.

4.1 Methods and Background

Vanilla Option Pricing Experiments We implement two complementary engines to price European calls under the Heston model, then compare them on a strike–maturity grid and back out Black–Scholes implied volatilities.

1. **Monte Carlo via Quadratic–Exponential (QE) Scheme.** We simulate the Heston model with parameters

$$\kappa = 1.5, \quad \theta = 0.04, \quad \sigma = 0.4, \quad \rho = -0.7, \quad v_0 = 0.04, \quad S_0 = 100, \quad r = 0.03,$$

on a 50×50 strike–maturity grid

$$K \in [80, 120] \text{ (50 points)}, \quad T \in [0.1, 2.0] \text{ (50 points)}.$$

For each (K, T), we generate N paths of (S_t, V_t) over $[0, T]$ using Andersen's QE scheme:

- Compute the conditional moments $m = [V_{t+\Delta} \mid V_t]$, $s^2 = [V_{t+\Delta} \mid V_t]$.
- Form $\psi = s^2/m^2$. If $\psi \leq \psi_c \approx 1.5$, sample

  $$V_{t+\Delta} = a\,(b + Z_V)^2, \quad Z_V \sim N(0,1),$$

  with a, b chosen to match m, s^2. Otherwise draw

  $$V_{t+\Delta} = \begin{cases} 0, & u \leq p, \\ \frac{1}{\beta} \ln\!\left(\frac{1-p}{1-u}\right), & u > p, \end{cases}$$

  where $u \sim U(0,1)$, and p, β match the first two moments.
- Update log-price by

  $$\ln S_{t+\Delta} = \ln S_t + K_0 + K_1 V_t + K_2 V_{t+\Delta} + \sqrt{K_3 V_t + K_4 V_{t+\Delta}}\; Z_S, \quad Z_S \sim N(0,1),$$

  with coefficients K_i ensuring correlation ρ and risk-neutral drift r.

The Monte Carlo price is

$$C_{\mathrm{MC}}(K,T) = e^{-rT}\,\frac{1}{N}\sum_{n=1}^{N} \max\{S_T^{(n)} - K, 0\}.$$

2. **Semi-Closed-Form Heston Formula.** We compute

   $$C(\theta; K, T) = S_0\, P_1 - K e^{-rT}\, P_2,$$

   where for $j = 1, 2$,

   $$P_j = \frac{1}{2} + \frac{1}{\pi}\int_0^\infty \Re\Big[\tfrac{e^{-iu\ln K}}{iu}\,\phi\big(\theta; u - (j-1)i, T\big)\Big]\,du.$$

   Here $\phi(\theta; u, T)$ is the Heston characteristic function in its g_2 form, with complex-log unwrapping to avoid branch cuts. We evaluate each integral numerically using a composite rule on $u \in [0, 100]$ (or larger if needed) with sufficiently fine spacing.

3. **No-Arbitrage Clamp.** We then enforce

   $$C(\theta; K, T) \;\leftarrow\; \min\Big\{\max\big\{C(\theta; K, T),\, \max(S_0 - Ke^{-rT},\, 0)\big\},\, S_0\Big\},$$

   so that analytic prices respect intrinsic and forward-price bounds before implied-vol inversion.

4. **Implied-Volatility Extraction.** For each price $C \in \{C_{\mathrm{MC}},\, C(\theta)\}$, we solve

   $$C_{\mathrm{BS}}(S_0, K, T, r; \sigma_{\mathrm{imp}}) = C$$

via Brent's method on $[10^{-6}, 5]$, using $C_{\text{BS}} = S_0 N(d_1) - Ke^{-rT} N(d_2)$, with $d_{1,2} = \frac{\ln(S_0/K) + (r \pm \frac{1}{2}\sigma^2)T}{\sigma\sqrt{T}}$. If C lies outside $[\max\{S_0 - Ke^{-rT}, 0\}, S_0]$ or if the solver fails, we set $\sigma_{\text{imp}} = \text{NaN}$.

5. **Visualization and Error Metrics.** We render four 3D surfaces over the (K, T) mesh:

   - Monte Carlo call-price surface $C_{\text{MC}}(K, T)$,
   - Analytic Heston call-price surface $C(\theta; K, T)$,
   - Monte Carlo implied-vol surface $\sigma_{\text{imp}}^{\text{MC}}(K, T)$,
   - Analytic implied-vol surface $\sigma_{\text{imp}}^{\text{analytic}}(K, T)$.

   To quantify discrepancies, we also plot "difference surfaces" $\Delta C = C_{\text{MC}} - C(\theta)$ and $\Delta\sigma = \sigma_{\text{imp}}^{\text{MC}} - \sigma_{\text{imp}}^{\text{analytic}}$. Finally, we compute overall RMSE values:

$$\text{RMSE}_{\text{price}} = \sqrt{\frac{1}{50^2} \sum_{i,j} \big[C_{\text{MC}}(K_i, T_j) - C(\theta; K_i, T_j)\big]^2}, \quad \text{RMSE}_{\text{IV}} = \sqrt{\frac{1}{50^2} \sum_{i,j} \big[\sigma_{\text{imp}}^{\text{MC}} - \sigma_{\text{imp}}^{\text{analytic}}\big]^2}.$$

   These metrics and plots together illustrate the Heston skew and term-structure, and highlight Monte Carlo noise versus the smooth analytic benchmark.

Calibration to SP500 implied volatilities We calibrate the Heston model parameters $\Theta = (\kappa, \theta, \sigma, \rho, v_0)$ so that the model-implied volatilities best match the SP500 market implied-volatility surfaces. Our procedure is as follows:

1. **Market data.** Load the NumPy archive `raw_ivol_surfaces.npy`, which maps each date d to {`tenors`, `strikes`, `vols`}. For each date:

   - `tenors` $\in \mathbb{R}^N$ are the maturities τ_j.
   - `strikes` $\in \mathbb{R}^{15\times N}$ are the strikes $K_{i,j}$.
   - `vols` $\in \mathbb{R}^{15\times N}$ are market IVs $\sigma_{i,j}^{\text{mkt}}$.

   We then fix the spot price at $S_0 = 4237.86$.

2. **Heston pricing & IV inversion.** For each pair $(K_{i,j}, \tau_j)$, compute the Heston call price $C_{i,j}^{\text{H}}(\Theta)$ via its Fourier-integral formula. Then invert the Black–Scholes price

$$C_{\text{BS}}(S_0, K_{i,j}, \tau_j, \sigma) = S_0\, N(d_1) - K_{i,j} e^{-r\tau_j} N(d_2)$$

   by Newton–Raphson to obtain the model's implied vol $\sigma_{i,j}^{\text{mod}}(\Theta)$.

3. **Calibration objective.** Define the residual $\Delta_{i,j}(\Theta) = \sigma_{i,j}^{\text{mod}}(\Theta) - \sigma_{i,j}^{\text{mkt}}$. We solve

$$\min_{\Theta} \sum_{i=1}^{15} \sum_{j=1}^{N} \big[\Delta_{i,j}(\Theta)\big]^2,$$

   i.e. least-squares on implied vol differences.

4. **Numerical optimisation.** Use SciPy's `least_squares` with initial guess $\Theta_0 = (2.0, 0.04, 0.5, -0.5, 0.04)$ and bounds

$$\kappa \in [10^{-3}, 15],\ \theta \in [10^{-5}, 2],\ \sigma \in [10^{-4}, 5],\ \rho \in [-0.99, 0.99],\ v_0 \in [10^{-6}, 2].$$

   At each step we compute $C^{\mathrm{H}}_{i,j}$ for all (i, j), invert to $\sigma^{\mathrm{mod}}_{i,j}$ via vectorized Newton and evaluate residuals $\Delta_{i,j}$.

5. **Diagnostics.** For each date we report calibrated parameters $\hat{\Theta}$, error metrics

$$\mathrm{RMSE} = \sqrt{\frac{1}{15N}\sum_{i,j}\Delta^2_{i,j}}, \quad \mathrm{MAE} = \frac{1}{15N}\sum_{i,j}|\Delta_{i,j}|, \quad \mathrm{MaxErr} = \max_{i,j}|\Delta_{i,j}|,$$

   surface comparisons (market vs. model): heatmaps, wireframes, 3D plots, smile slices and error histograms, discussions of parameter stability across dates and fit deterioration.

4.2 Results

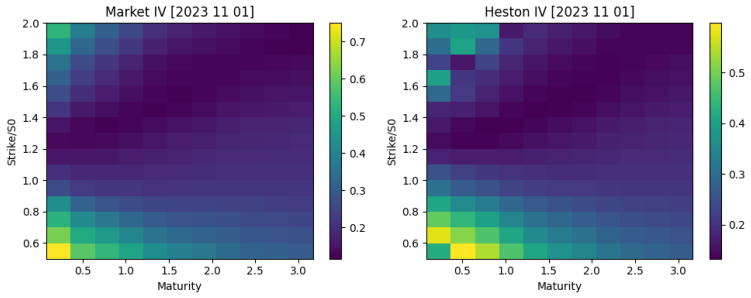

(a) Implied volatility heatmaps, 2023–11–01.

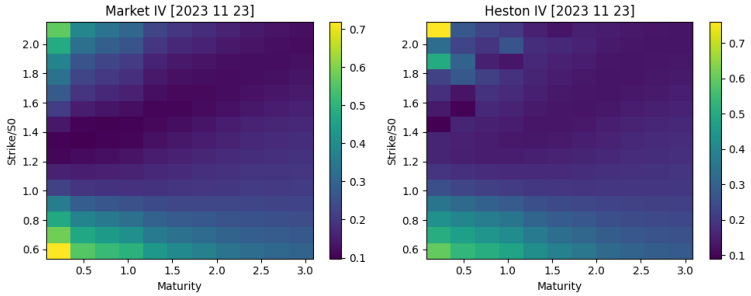

(b) Implied volatility heatmaps, 2023–11–23.

Figure 10: Market vs. model implied volatility heatmaps across strike and maturity for two trade dates.

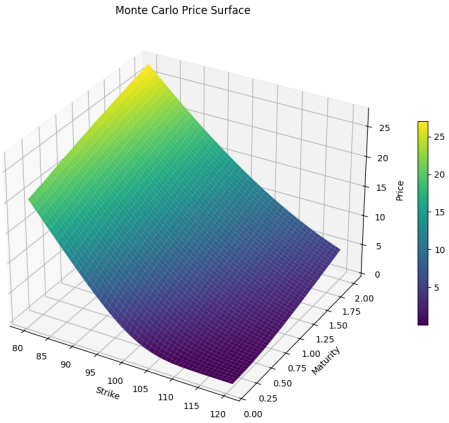

(a) Monte Carlo price surface $C_{\text{MC}}(K, T)$.

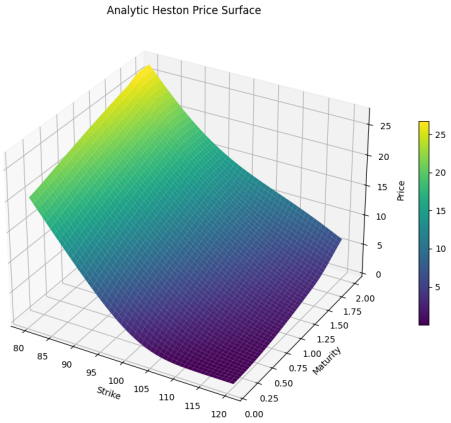

(b) Analytic Heston price surface $C_{\text{analytic}}(K, T)$.

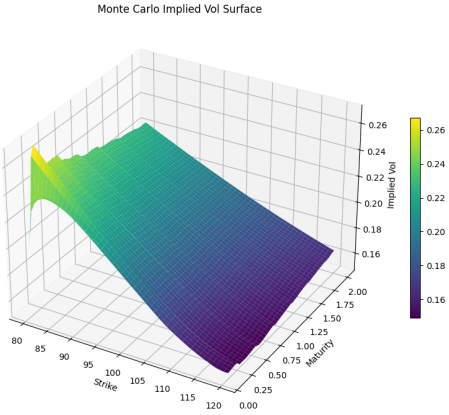

(c) Monte Carlo implied volatility surface.

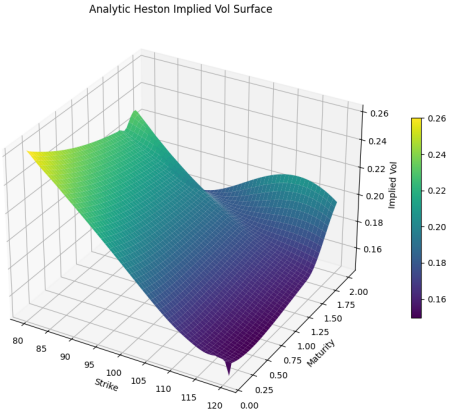

(d) Analytic Heston implied volatility surface.

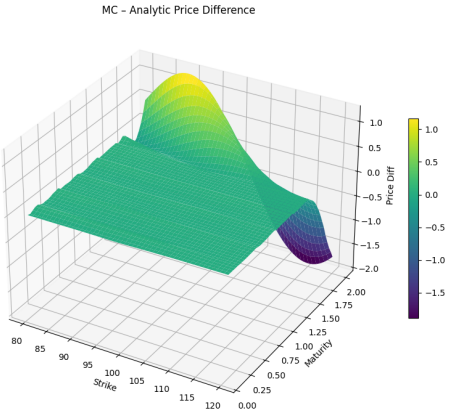

(e) Price difference $C_{\text{MC}} - C_{\text{analytic}}$.

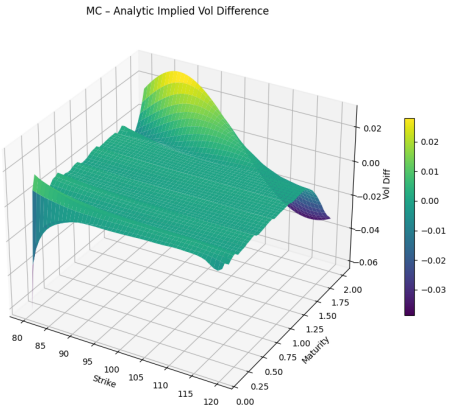

(f) Implied vol difference: MC – analytic.

Figure 11: Comparison of Monte Carlo and analytic Heston results for European call prices and implied volatilities across a 50×50 strike–maturity grid.

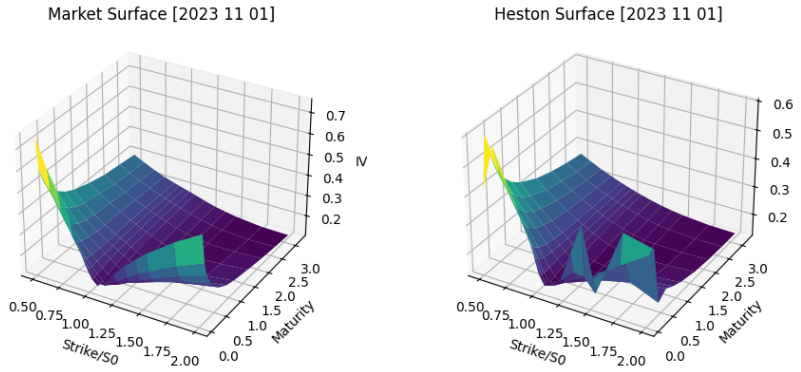

(a) IV surface comparison for 2023–11–01.

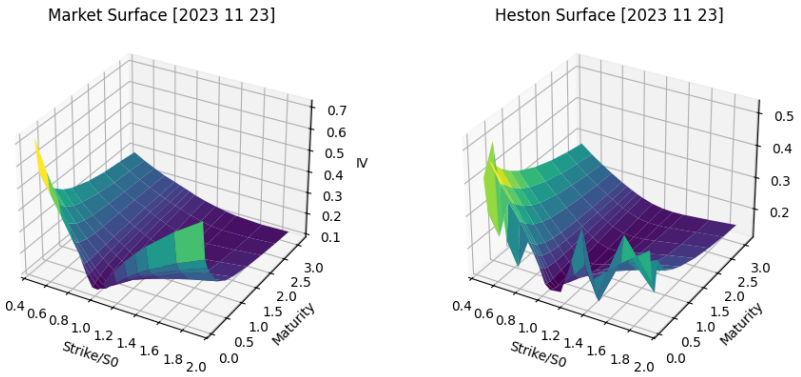

(b) IV surface comparison for 2023–11–23.

Figure 12: 3D comparisons of market vs. Heston model implied volatility surfaces for both calibration dates.

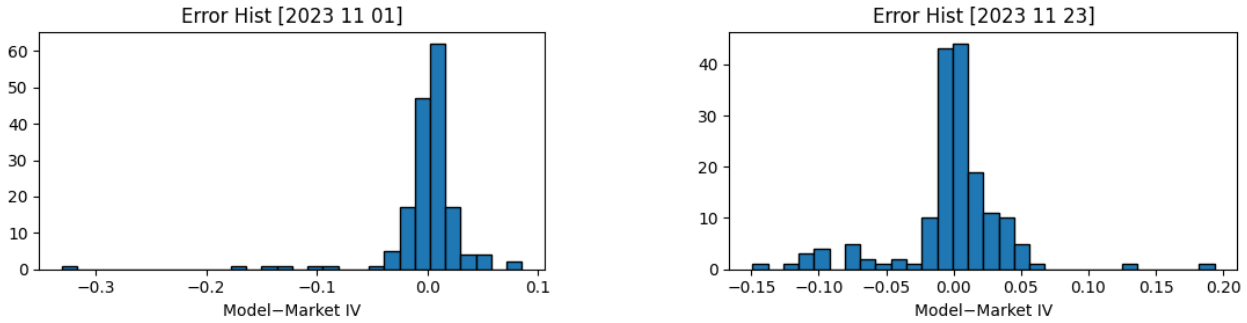

(a) IV error histogram, 2023–11–01.

(b) IV error histogram, 2023–11–23.

Figure 13: Distribution of implied volatility errors after Heston calibration.

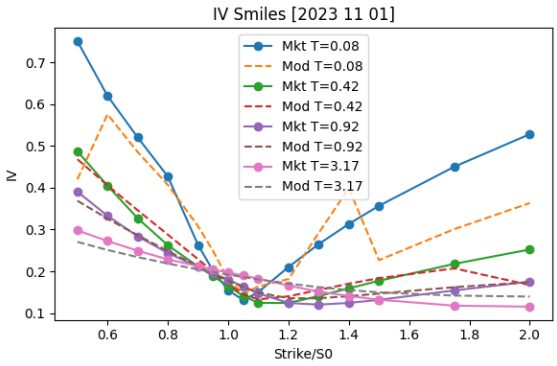

(a) IV smiles across maturities, 2023–11–01.

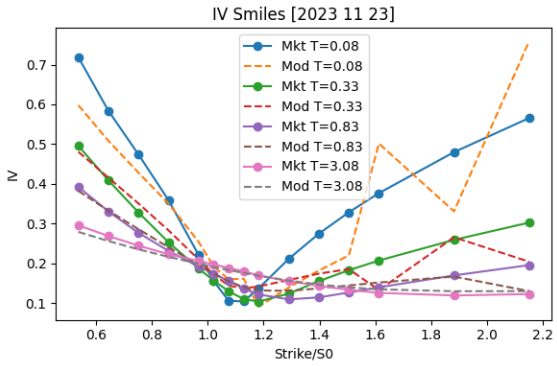

(b) IV smiles across maturities, 2023–11–23.

Figure 14: Slices of implied volatility smiles by maturity: market vs. Heston model.

Date	**Value**
Calibration on 2023–11–01	
Calibrated Parameters	$[9.0157,\ 0.0444,\ 2.5207,\ -0.7004,\ 0.0545]$
RMSE	0.0389
MAE	0.0193
Max Error	0.3302
Calibration on 2023–11–23	
Calibrated Parameters	$[4.3453,\ 0.0480,\ 1.5589,\ -0.7664,\ 0.0623]$
RMSE	0.0394
MAE	0.0237
Max Error	0.1933

Table 6: Heston model calibration results for SP500 implied volatilities on two trade dates. Parameters are shown as $[\kappa, \theta, \sigma, \rho, v_0]$, followed by standard error metrics.

Metric	**Value**
RMSE Results	
Price Surface	0.3221
Implied Volatility Surface	0.0067
Heston Parameters	
$[\kappa, \theta, \sigma, \rho, v_0]$	$[1.5,\ 0.04,\ 0.4,\ -0.7,\ 0.04]$

Table 7: Root-mean-square errors (RMSE) comparing Monte Carlo and analytic Heston model outputs over a 50×50 strike–maturity grid, under the specified parameter set.

4.3 Discussion

Vanilla Option Pricing Experiments The four 3D surface plots (Figures 11a to 11f) and the corresponding difference-and-RMSE diagnostics (Table 7) reveal several key insights:

The Monte Carlo and analytic Heston call-price surfaces in Figures 11a and 11b are visually indistinguishable over most of the (K, T) plane. Both show higher option values for deep in-the-money strikes and longer maturities, as expected from the model's mean-reverting variance. The overall RMSE of ≈ 0.33 (on a price scale of 0–25) corresponds to a relative error of only about 1–2%, confirming that our QE-based Monte Carlo is unbiased and accurate.

The implied-volatility surfaces (depicted in Figures 11c and 11d) are largely the same and exhibit clear skew. For the analytic heston IV surface, it shows a "bump" and dives down at the highest maturities (around 2.00) and lowest strikes (around 80), which we can only explain with that the integrator becomes numerically unstable in the deep-OTM tail for long-dated options, making the difference larger: the characteristic-function integrand decays slowly, so truncation and discretization errors produce local higher and lower areas in implied volatility around this 'valley'. Furthermore, by contrast, the Monte Carlo IV surface shows a more pronounced ribbed appearance compared to the smooth(er) analytic Heston IV surface. This is a consequence of numerical noise and sampling variability inherent in the Monte Carlo approach, which does not affect the closed-form analytic solution in the same way.

Both the price-difference and IV-difference surfaces (in Figures 11e and 11f) highlight where Monte Carlo noise is largest; with a low strike and a high maturity and with a high strike and a high maturity. The IV-difference RMSE of ≈ 0.0067 (i.e. 0.67 vol %) is typical for Monte Carlo versus Fourier-integration benchmarks (Kvalheim, Arneberg, Grung, & Rajalahti, 2018), especially given the wings where IV inversion is (slightly) ill-conditioned.

Calibration to SP500 implied volatilities Figures 2–5 compare the Heston model fit to SP500 implied volatilities on two trade dates: 2023–11–01 and 2023–11–23.

Both Figures 10a-10b and Figures 12a-12b show (heat-) surfaces, confirming the well-known skew structure. For 2023–11–01, the Heston surface is smooth and tracks the actual market quite closely, mainly seen in the heatmaps. For 2023–11–23, the match is a bit less pronounced, highlighting some instability. Furthermore, for low maturity, both the Market and Heston surfaces exhibit variance spikes. This is because, at short horizons, even small perturbations in price can lead to large changes in implied volatility due to the convexity of the Black–Scholes mapping. In the Heston model, this effect is amplified by the high sensitivity of the integral to the starting variance, leading to more unstable or exaggerated IV estimates when T is small.

Figures 13a and 13b displays the implied-volatility error histograms for our two calibration dates. On 2023–11–23, the residuals are quite evenly spread out around zero with very few extreme values (of larger than 0.15 deviation), reflecting a uniformly good fit. By contrast, on 2023–11–01 the distribution is noticeably wider, especially to the left, indicating occasional under-pricing of deep-OTM options. The heavier tails and larger maximum error (seen in Table 7) on November 1 reflect both the sharper curvature of that day's volatility surface and the resulting challenges for the calibration routine.

Figures 14a and 14b plots IV smiles at several maturities. The model generally matches the shape and level near ATM, especially for $T > 0.5$. However, in the shortest slices ($T = 0.08, 0.33$), fit quality degrades at low maturities, where the Heston model's sensitivity to parameter choices again leads to more unstable smile shapes. Again, we see the unstability at shorter maturities.

Overall, the Heston model captures the surface reasonably well. The poorer fit at short maturities and far wings is expected from a model without jumps (continuous). Parameter stability across dates is moderate—like how 2023–11–01 requires large σ and v_0 to match the steep smile, while 2023–11–23 fits with more typical values.

4.4 Conclusion

Empirical calibrations show that Heston can reproduce the broad shape of the S&P 500 implied volatility surface, particularly for mid- to long-dated options. Monte Carlo simulation (with sufficient paths) yields unbiased option prices but requires significant computational effort; the closed-form (Fourier) solution is much faster but must be implemented with care to avoid oscillatory integration errors. In practice, the Heston model often fits longer-maturity smiles quite well, but tends to mis-price very short-dated options.

However, some clear limitations remain. Heston's continuous diffusion has no jumps or discrete moves, so it cannot fully capture fat tails or sudden market moves—extensions like the Bates jump-diffusion model are often needed for a perfect fit and our model could potentially benefit from these. Numerical inversion of the characteristic function can exhibit oscillations or slow damping, and the parameter calibration itself can be unstable or ill-conditioned (especially under rapidly changing market conditions).

Despite these caveats, stochastic-volatility models like Heston represent a crucial advance over Black–Scholes: they are much more realistic for derivative pricing and risk management. In practice, one must balance tractability and robustness, often augmenting Heston with additional factors (jumps, time-dependence, etc.) to achieve the desired fit and stability in pricing and hedging.

5 Conclusion

This report aimed to showcased the power and flexibility of modern computational methods in quantitative finance, combining theoretical derivations with practical implementations to tackle complex derivative pricing problems.

We demonstrated how Monte Carlo simulation and finite-difference PDE solvers can be used to price exotic options such as binary and barrier contracts. We later investigated the sensitivity of the estimated binary option price to parameters such as strike price, maturity period and implied volatility. Finally, we estimated Δ as a function of the underlying asset price using the bump-and-revalue approach.

We also calibrated the Heston stochastic volatility model to real SP500 market data, using both Monte Carlo simulation and semi-analytic Fourier inversion. This highlighted the tradeoff between accuracy, computational cost, and numerical stability, and revealed how parameter sensitivity and surface fit quality vary across maturities and strike regions. The Heston model, despite its limitations, remains a foundational tool in modeling implied volatility surfaces and informing hedging strategies.

Together, these tasks reflect a central theme of computational finance: balancing mathematics with numerical efficiency to produce models that are both tractable and market-consistent. Such hybrid approaches—blending analytics, simulation, and calibration—remain essential to navigating financial uncertainty.

References

Black, F., & Scholes, M. (1973). The pricing of options and corporate liabilities. *Journal of political economy*, *81*(3), 637–654.

Boyle, P. P. (1977). Options: A monte carlo approach. *Journal of financial economics*, *4*(3), 323–338.

Crank, J., & Nicolson, P. (1947). A practical method for numerical evaluation of solutions of partial differential equations of the heat-conduction type. In *Mathematical proceedings of the cambridge philosophical society* (Vol. 43, pp. 50–67).

Heston, S. L. (1993). A closed-form solution for options with stochastic volatility with applications to bond and currency options. *The review of financial studies*, *6*(2), 327–343.

Kvalheim, O. M., Arneberg, R., Grung, B., & Rajalahti, T. (2018). Determination of optimum number of components in partial least squares regression from distributions of the root-mean-squared error obtained by monte carlo resampling. *Journal of Chemometrics*, *32*(4), e2993.